DOI: 10.1002/smll.200700334

Magnetophoretic Continuous Purification of Single-Walled Carbon Nanotubes from Catalytic Impurities in a Microfluidic Device

*Joo H. Kang and Je-Kyun Park**

A magnetophoretic continuous purification method is presented of single-walled carbon nanotubes (SWCNTs) from the superparamagnetic iron-catalyst impurities in a microfluidic device without any influence on inherent SWCNT properties. By employing microfluidics and a magnetic-field-induced saw-tooth nickel microstructure, a highly enhanced magnetic force in adjoining microchannels is exploited. The iron impurities of SWCNTs are attracted towards areas of higher magnetic-flux density in the microchannels where magnetic field was asymmetrically generated perpendicularly to the streamline. We obtained highly purified SWCNTs at a rate of 0.36 mg h^{-1} and that are estimated to be about 99 % purity.

Keywords:
- carbon nanotubes
- magnetophoresis
- microfluidics
- purification
- separation

1. Introduction

Single-walled carbon nanotubes (SWCNTs) have been investigated for their promising wide applications.[1,2] Current methods for the synthesis of SWCNTs make use of metal catalysts such as Fe, Ni, and Co, which need to be removed for many potential applications. There have been many considerable reports about CNTs purification methods, such as gas-phase oxidation, wet-chemical and thermal treatment, microwave-assisted methods, and combined multistep purification platforms.[3,4] Despite the successful removal of metal impurities from SWCNTs, current purification methods, mainly using chemical, thermal, and ultrasonic treatments, give rise to structural defects or surface modification of SWCNTs.[4] Fortunately, most metal catalysts for SWCNT synthesis are superparamagnetic nanoparticles[5] and several researches have come forward to purify SWCNTs using a magnetic-trapping method.[6–8] However, the magnetic purification schemes were only demonstrated on a test-tube scale and they were devoid of the precise fluidic control and enhanced magnetic force, which limits highly effective purification. This is because the metal impurities of SWCNTs are superparamagnetic nanoparticles having small magnetic susceptibility and consequently cause the weak magnetophoretic force.

As lab-on-a-chip technology has developed, microfluidic applications have extended to diverse research fields including biology,[9] materials science,[10] and other interdisciplinary realms.[11,12] Recently, SWCNTs have been employed in microfluidic devices for SWCNT patterning,[13] chemical analysis,[14,15] and size differentiation of CNTs.[16,17] These recent works show that microfluidic techniques are expected to contribute significantly to future CNT development. Magnetophoretic techniques also have been dedicated to miniaturized magnetophoretic devices for magnetophoretic immunoassays[18] and magnetic-particle separation,[19] which offer highly efficient and sensitive magnetophoresis.

Here, we demonstrate magnetophoretic purification of SWCNTs from superparamagnetic metal impurities in a microfluidic device, which provides the capability to control the SWCNT-containing fluid and the highly enhanced magnetic force acting on the metal impurities, giving efficient magnetophoresis in microchannels. The microfluidic device offers chemical- or gas-free purification of SWCNTs as well as a universal platform that can be applied to purify various

[*] J. H. Kang, Prof. J.-K. Park
Department of Bio and Brain Engineering
Korea Advanced Institute of Science and Technology (KAIST)
335 Gwahangno, Yuseong-gu, Daejeon 305-701 (Korea)
Fax: (+82) 42-869-4310
E-mail: jekyun@kaist.ac.kr

small NANO MICRO

types of CNTs if they have paramagnetic metal catalysts. In addition, our microfluidic purification method has several advantages: low cost, high purity, and continuous single-step, defect-free purification.

2. Design and Simulation

2.1. Device Design

Figure 1a illustrates the continuous magnetophoretic purification of superparamagnetic metal catalysts in SWCNTs. As the raw SWCNT solution passes through the magnetic-field-applied microchannel, Fe nanoparticles in SWCNTs are laterally deflected towards areas of higher magnetic-flux density, while the pure SWCNTs keep their flow path and are finally obtained though outlet 4 in Figure 1b. The device consists of a single inlet, four outlet ports, and a 2.5-cm-long microfluidic separation channel. We designed four outlet ports considering purification throughput, estimated purity of the collected SWCNTs, and the capability of a syringe pump. As the number of outlet ports increases, overall purification throughput decreases, while as that decreases, the achieved purity can be reduced.

Two types of microfluidic device were designed to have 100- and 1000-μm-wide microchannels, where the height of the channel was commonly 50 μm (Figure 1c). The device of 100-μm width was used for fluorescence analysis for observing magnetophoretic migration. The microchannel for continuous purification was designed to have a width of 1000 μm to prevent the microchannel being plugged because the SWCNT solution injected into the microfluidic device still had some bundles of nanotubes even after dispersion procedure. The bundles of SWCNTs have a larger magnetophoretic force and a more severe microfluidic shear force than a single-dispersed SWCNT. Therefore, the shear force removes them efficiently by sweeping with flow. Also, we adopted a design using a single inlet and four branched-off outlets for collecting purified SWCNTs, where outlet 4 for pure SWCNTs has a largely expanded channel to prevent contamination between the purified SWCNTs and the impurities caused by occasional fluidic fluctuation during the long-time purification (Figure 1b). Once the Fe impurities come into outlet 4, they are attracted to the higher magnetic-flux density (B) region and are locally confined because the slowed linear velocity makes a net force between magnetic and fluidic shear forces inclined toward a magnetic-energy source.

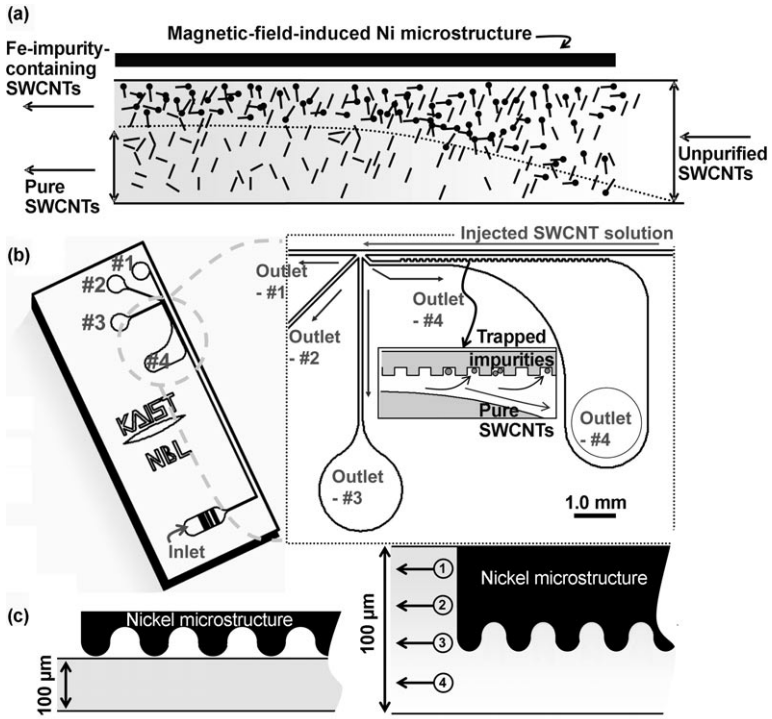

Figure 1. Design of a magnetophoretic SWCNT purification device. a) Continuous magnetophoretic purification of SWCNTs in a microfluidic channel. Injected as-prepared SWCNTs migrate to areas of higher magnetic-flux density. When the flow stream branches out near the outlet ports, we can continuously separate the pure SWCNTs from the impurity-containing SWCNTs. b) The device consists of single inlet port and four outlet ports. In particular, outlet 4 has an expanded channel to slow the flow rate to attract the impurities caused by incidental failure of fluidic control. The irregular microchannel wall by outlet 4 was employed to collect impurities caused by incident microfluidic fluctuation, keeping the trapped impurities from sweeping up with the fluidic shear force. c) We designed several types of microfluidic device to optimize the magnetophoretic separation condition of SWCNTs varying the microchannel width and the alignment of the microchannel and the nickel structure.

2.2. Magnetic-Field Simulation

The device has a ferromagnetic-nickel microstructure for enhancement of the magnetic-flux-density gradient (∇B)[20] across the microfluidic channel (Figure 2). Compared to a magnetic field without a nickel microstructure, the magnetic-flux-density gradient is much larger near to the nickel microstructure and the effect of the ferromagnetic microstructure becomes negligible behind 300 μm from the nickel microstructure. This indicates that impurities need to pass through an area that is closer than about 300 μm to the magnetic-field-induced nickel microstructure. Therefore, the ferromagnetic nickel microstructure was aligned to be placed 300 μm apart from the microchannel (Figure 1c); here a flow velocity larger than that of the microchannel sidewall, generated in a hyperbolic flow profile, prevents magnetically confined and

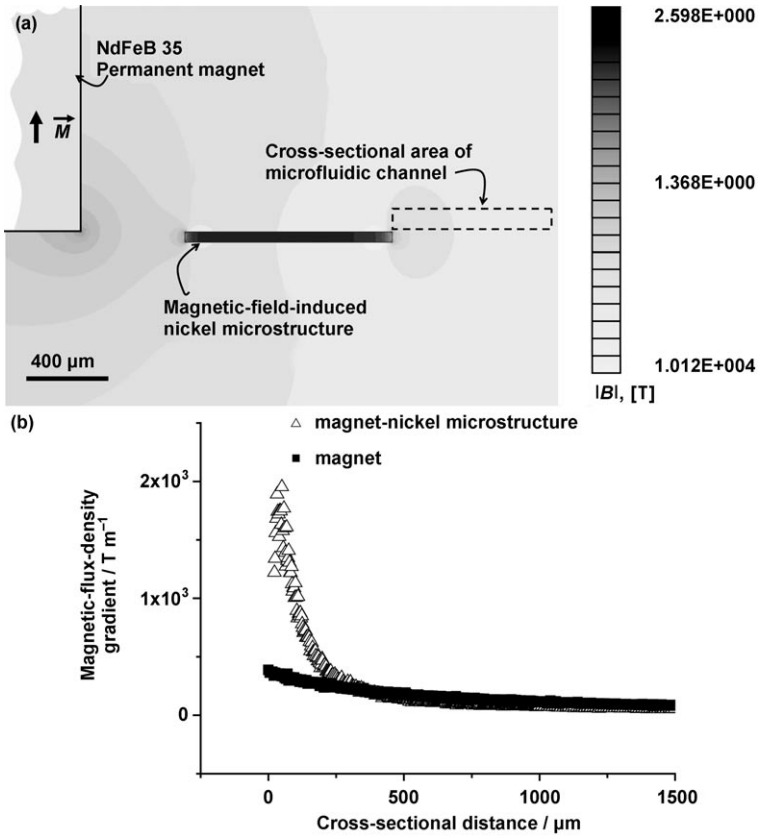

Figure 2. Numerical analysis of the enhanced ∇B at the cross section of the microfluidic device to evaluate the effect of the nickel microstructure (solved by the finite element method magnetics (FEMM) program). Plot of dB/dx against distance from the nickel microstructure, (b) is collected from the cross-sectional area of microchannel in (a). Around the nickel microstructure, the magnetic-flux-density gradient is much larger than that without nickel microstructure. Beyond 300 μm from the nickel, the influence of nickel for the enhancement of dB/dx is negligible. Therefore, impurities need to pass through the area that is closer than about 300 μm from the magnetic-field-induced nickel microstructure.

flocculated impurities from clogging the microchannel. We designed a nickel microstructure to have a saw-tooth edge to provide the repeated highly enhanced ∇B along the microfluidic channel.[21] Magnetic field and electric field are analogous in converged field lines in the vicinity of the edges of the energy source and a highly enhanced electric field at the edge of the saw-tooth electrodes was reported for cell lysis.[22] Therefore, we designed a saw-tooth ferromagnetic microstructure for the enhancement of the magnetic-energy gradient around the microstructure.

3. Results and Discussion

3.1. Fluorescence Measurements of Magnetophoretic Analysis

To confirm the mass transport of impure SWCNTs driven by magnetic force, the center-focused raw SWCNT solution were, by using the sheath flow of fluorescein solution (3.0 mM), deflected to the area of higher magnetic-flux density causing reduced fluorescence intensity at that region (Figure 3). When the fluorescence intensity was measured around the outlet channels we observed that the SWCNTs were diffused away from the center-focused SWCNT flow without applied magnetic field (Figure 3b). However, after developing a magnetic-flux-density gradient across the microchannel, iron-impurity-containing SWCNTs were migrated to the higher-magnetic-flux-density area (the right direction in Figure 3c), giving an asymmetric fluorescence intensity across the microchannel. Figure 3c shows that the magnetophoresis of the impurities overwhelms the spontaneous mass transport of SWCNTs driven by the concentration gradient. The magnetic property of SWCNTs is reported as diamagnetic except for the case of metallic SWCNTs in the tube-axis direction of magnetic field[23] and superparamagnetic iron nanoparticles. Because the magnetic susceptibility of iron nanoparticle is even larger than the absolute value of diamagnetic susceptibility of SWCNTs, the magnetic mobility of impurity-containing SWCNTs is positive. Therefore, as shown in Figure 3c, impure nanotubes are attracted to the higher-magnetic-field region.

3.2. Magnetically Confined Impurity-Containing SWCNTs

Figure 4 shows the locally confined iron-containing SWCNTs on the channel sidewall induced by the enhanced magnetic field. Locally confined impure SWCNTs were repeatedly concentrated in the regions of highest magnetic-flux density. We can confirm that this local concentration of SWCNTs was chiefly caused by magnetic force, observing the release of SWCNTs as the magnetic field was removed. The magnetically confined impurity-containing SWCNTs revealed that the magnetic force near the nickel microstructure, holding the metal-impurity-containing SWCNTs, to be not less than the microfluidic shear force, $F_{shear} = \eta v_0 d^{-1}$, where η is the dynamic viscosity of water (0.89×10^{-3} kg m^{-1} s^{-1}), v_0 is the volumetric flow rate of the SWCNT solution, and d is the diameter of the channel. Calculated F_{shear} has $\approx$pN order and we can assume that the magnetic force, F_{mag}, attracting the iron-nanoparticle impurity is more than F_{shear}, and F_{mag} is rapidly reduced as the dis-

small NANO MICRO

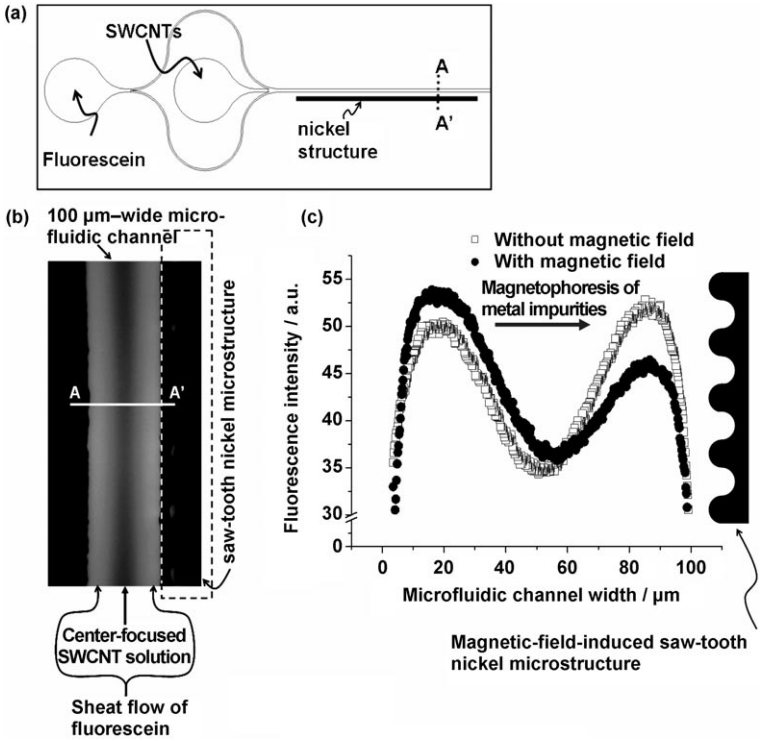

Figure 3. a) Fluorescence analysis was carried out to confirm the mass transport of impurity-containing SWCNTs driven by magnetic force using a microfluidic device. b) Fluorescence microscopy image of center-focused raw SWCNT solution in 100-μm-wide microchannel without applied magnetic field. c) Fluorescence analysis showing that the impurity-containing SWCNTs are deflected to the higher-magnetic-flux-density area causing the reduced fluorescein intensity at that region. The plotted data of (c) was obtained from the cross section *A*–*A*′ in (b) by averaging 10 different fluorescence intensity data with error less than 10% around the microchannel.

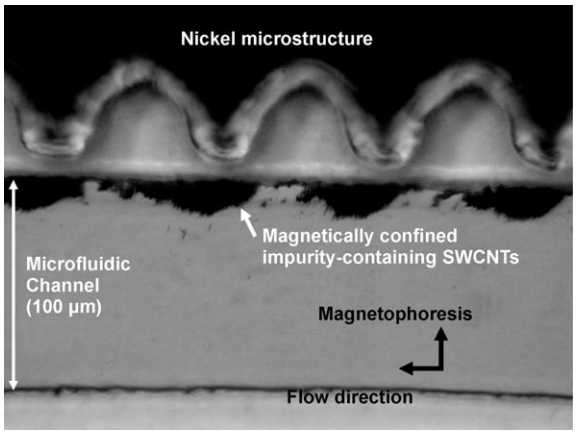

Figure 4. Magnetically confined impurity-containing SWCNTs on the sidewall of the saw-tooth nickel microstructure induced by a permanent magnet. Locally confined impure SWCNTs were repeatedly concentrated in the regions of highest magnetic-flux density.

tance from the magnetic-field-induced nickel microstructure increases. F_{mag} at the region several hundred micrometers apart from the nickel microstructure is expected to have ≈ pN order because F_{mag} (Equation (1)) is proportional to the product of B and dB/dx (Figure 2), where μ_o and $\Delta\chi$ are the vacuum permeability and the net magnetic susceptibility of impurity in aqueous solution, respectively.

$$F_{mag} = \frac{V\Delta\chi\nabla B^2}{2\mu_0} \quad (1)$$

3.3. Energy Dispersive X-ray Spectroscopy and Transmission Electron Microscopy Studies

Energy dispersive X-ray spectroscopy (EDS) results, shown in Figure 5 and Table 1, prove successful magnetophoretic purification, showing that the peak intensity for iron (Fe Ka at 6.403 keV) is highly reduced. In the EDS analysis, sodium, sulfur, and other elements were detected because the collected SWCNT sample, followed by methanol washing and drying processes, still had the remnant sodium dodecylbenzene sulfonate

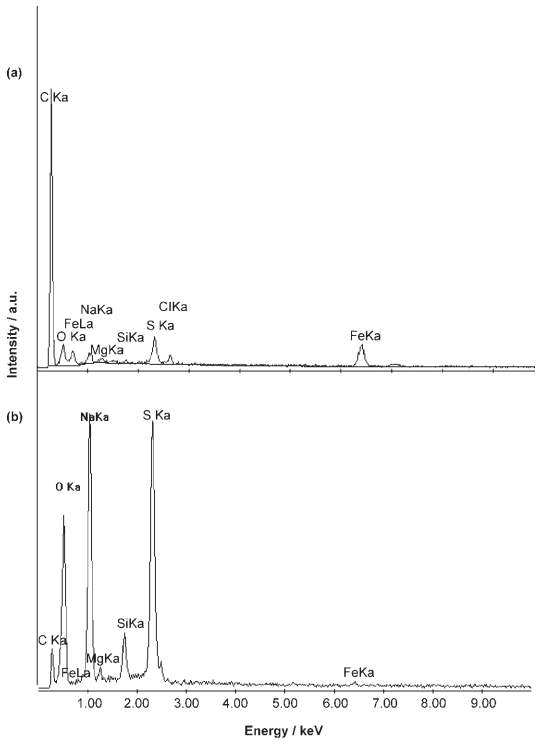

Figure 5. EDS results of a) as-received and b) purified SWCNTs.

Table 1. Elemental analysis of as-received and purified SWCNTs by EDS. The data were collected at 10 different points and averaged. SD: standard deviation.

	Unpurified		Purified	
	Average wt%	SD.	Average wt%	SD.
C K	75.49	3.63	17.81	5.44
O K	8.71	2.66	36.38	1.65
Na K	1.95	0.85	23.7	2.34
Mg K	0.44	0.11	1.17	0.16
Si K	0.47	0.22	1.94	0.62
S K	3.27	1.24	17.93	3.54
Fe K	9.87	2.22	0.97	0.18

(NaDDBS) surfactant and impurities of its own. Although EDS results show highly reduced iron content in the purified sample, they do not present determinate quantitative results because not only can we not assure the uniform thickness, density, and geometric feature of the prepared samples but also we need the *k* factor for quantitative calibration according to the Cliff–Lorimer equation.[24] Determination of the *k* factor requires the impurity content of the SWCNTs to be dispersed by surfactant (NaDDBS), which can be obtained by thermogravimetric analysis (TGA). Although we have tried to analyze SWCNTs using TGA, we had a problem in that the surfactant contains its own impurities or some components affecting the TGA process so that we cannot discriminate weight percent of SWCNTs from the impurities of surfactant. Moreover, recent papers on SWCNT purification presenting TGA results commonly used acid solution or organic solution, such as *N*,*N*-dimethylformamide (DMF) or toluene, in which solubility of SWCNTs is quite small. Therefore, we reached the conclusion that TGA was not an adequate method for our system and also that the consequent EDS study based on the *k* factor cannot present accurate quantitative results on the purity.

After the surfactant was removed, as-dispersed and magnetically purified SWCNTs were observed by transmission electron microscopy (TEM), as shown in Figure 6. The results of this study also provide proof of the successfully purified SWCNTs through the microfluidic channels under the applied magnetic field.

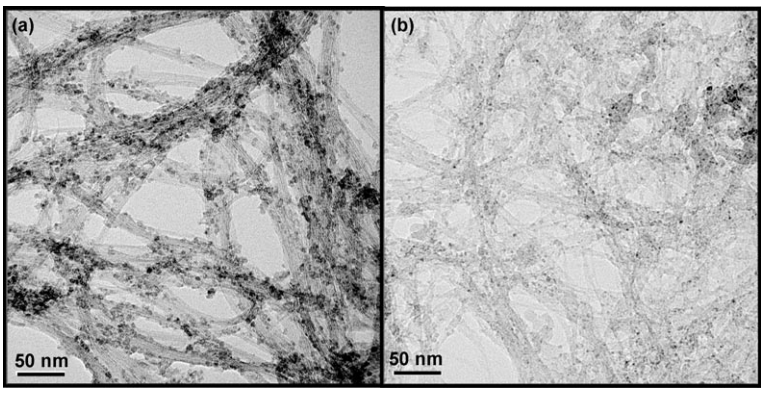

Figure 6. TEM images of a) as-dispersed and b) magnetophoretically purified SWCNTs.

3.4. Magnetic Characterization of Superparamagnetic Impurities

The *M*–*H* curves of as-prepared and purified SWCNTs (about 10.0 mg) measured by superconducting quantum interference device (SQUID) magnetometry at 300 K also support that the purified SWCNTs rarely have superparamagnetic iron impurities (Figure 7). In our system, the saturation magnetic moment (M_S) should be calibrated to the net weight of SWCNTs because the purified SWCNTs are mixed with surfactant. The measured moment was 8.37×10^{-4} emu where the sample weight was 11.9 mg. Considering the dilution ratio between the SWCNTs and surfactant (1:5), we obtained the calibrated M_S of 0.422 emu g^{-1} through the simple calculation, $(8.37\times10^{-4}\ \text{emu})/(11.9\times10^{-3}\ \text{g}/6)$, which is rather smaller than that of SWCNTs having $98.474\pm0.33\,\%$ of the purity.[5] The practical M_S can be smaller than calibrated since the dilution factor (1/6) increases if the collected SWCNTs are washed with methanol. Comparing our result with the previous report,[5] we are able to estimate the purity of the purified SWCNTs to be around 98–99%.

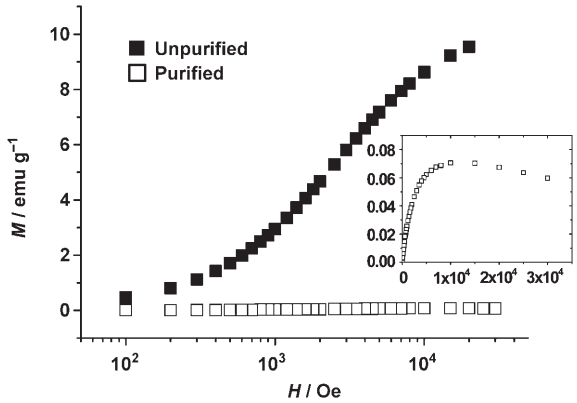

Figure 7. *M*–*H* curve of SWCNTs measured at 300 K using SQUID magnetometry proves that magnetically purified SWCNTs have remarkably reduced iron content, showing the decreased magnetic susceptibility. The inset shows a magnified graph of purified SWCNTs below 0.1 emu g^{-1} of magnetization.

NANO MICRO small

The purification throughput depends on the solubility of SWCNTs in water. This purification method resulted in a yield of about 10.1%, which is less than that of 25% obtained by only magnetic filtration.[6] As the solubility is increased up to $\approx 20\ mg\,mL^{-1}$,[25] a larger amount of SWCNTs can be continuously purified in the magnetophoretic device. Although the present results were obtained using as-received SWCNTs encapsulating iron-nanoparticles catalysts, we can achieve a higher yield of the purified SWCNTs by using the mechanical removal method[7] of metal catalyst embedded in SWCNTs followed by our magnetophoretic purification method. Moreover, a second round of purification using the purified SWCNTs will improve the purity because we demonstrated the magnetophoretic purification in a first round using as-received SWCNTs. However, the recovery yield of purified SWCNTs is relatively lower than other chemical purification methods since the magnetophoretic purification conducts physical separation of pure SWCNTs from metal-catalyst-containing SWCNTs.

4. Conclusions

We have presented continuous magnetophoretic purification of high-pressure carbon monoxide (HiPco) SWCNTs from the iron-nanoparticle-containing SWCNTs in a microfluidic device. We used a saw-tooth nickel microstructure for enhancement of the magnetic-energy gradient, which was properly arranged within the microchannel and a permanent magnet to utilize the higher magnetic-flux-density gradient. Only by a single-round purification process, we obtained highly purified SWCNTs estimated to be about 98–99% from the as-received SWCNTs having about 18.14% of iron content. The continuous magnetophoretic purification in a microfluidic device can also be used for other types of nanomaterials that contain paramagnetic or superparamagnetic impurities. This report is not only the first demonstration of magnetic purification of CNTs in a microfluidic device but also shows a reliable microfluidic device working for several days without observing the purification process by a research operator. Our method can offer a process for fundamental studies and diverse applications using the unique magnetic properties of intrinsic CNTs.

5. Experimental Section

Materials: SWCNTs produced by the HiPco technique (Carbon Nanotechnologies Inc., USA) were used. The as-received SWCNTs contained 18.14 ± 0.79 weight% of Fe as a catalyst, which was analyzed by TGA three times. To obtain liquid-soluble SWCNTs, as-received SWCNTs were dispersed in deionized water using surfactant NaDDBS (about $1.0\ mg\,mL^{-1}$).[25] After ultrasonic treatment, the partially dispersed SWCNTs were left for an hour to induce sedimentation of large bundles of nanotubes. Finally, highly dispersed supernatant nanotubes were immediately used for magnetophoretic purification without further filtering or ultracentrifugation processes.

Microfabrication: The fabricated device consisted of microchannels and a nickel microstructure (Figure 8). The microchannel was prepared by a poly(dimethylsiloxane) (PDMS) micromolding method using a SU-8 2025 photoresist (PR). The nickel microstructure for the enhancement of ∇B was prepared by a nickel electroplating method using a THB 151N negative PR mold. Electroplating seed layers (Cr(200 Å)/Au(3000 Å)) were deposited by magnetron metal sputtering and a 100-μm-thick negative PR was patterned on Au-deposited glass wafers. After the electroplating process, a chemical mechanical polishing (CMP) step was followed to make the nickel structure have an even height of 50 μm. Electroplated nickel microstructures were fabricated in large quantities through a four-inch glass wafer and collected by detaching them from the wafers. The size of the nickel structure was 50 μm in height, 1 mm in width, and 25 mm in

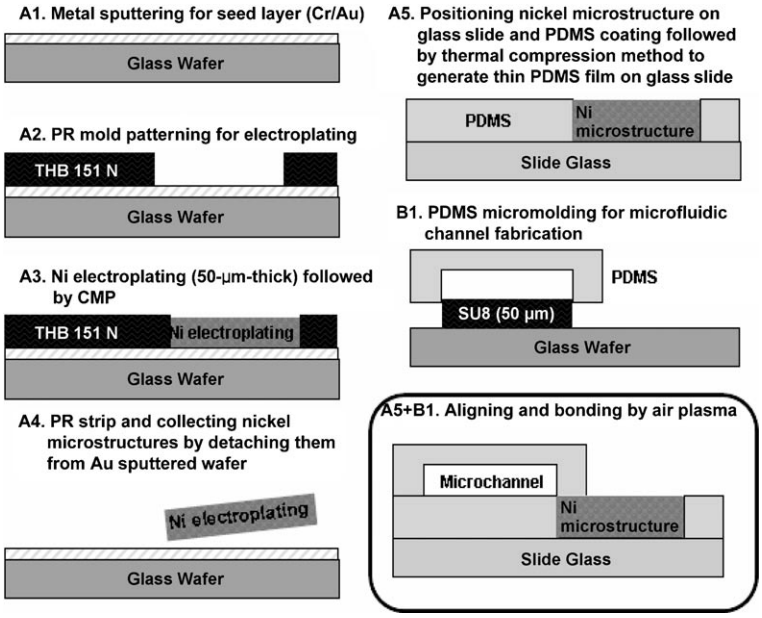

Figure 8. Fabrication process of microfluidic device for magnetophoretic purification of SWCNTs. The microfabrication process consists of PDMS micromolding and nickel electroplating. In the nickel electroplating step (A3), a CMP process ensured even height of nickel structures. After air plasma treatment of PDMS substrates, the microfluidic devices were accomplished by alignment between microchannels and nickel microstructures.

length. The protruding teeth of the saw-tooth nickel structure was 50 μm long and the distance between teeth was also 50 μm. Nickel microstructure was embedded in a 50-μm-thick PDMS film fabricated by a thermal-compression method. In the PDMS-film fabrication (A5 of Figure 9), the quantity of prepolymer consumed is so small that it is troublesome to prepare the mixture of prepolymer and curing reagent in a ratio of 10 to 1. To reduce such a tedious work, we kept the mixture of prepolymer in a refrigerator at -23°C and used the frozen prepolymer mixture. This freezing method preserves the prepolymer from curing for several months. The device fabrication was finished by bonding PDMS substrate with a glass slide containing a nickel microstructure (Figure 8, A5 + B1).

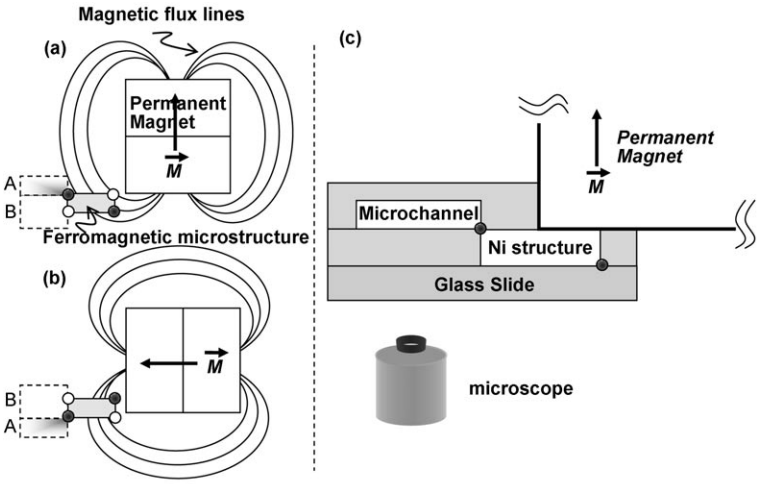

Figure 9. a, b) Schematic view of relationship between a permanent magnet and a ferromagnetic microstructure positioned nearby a permanent magnet. According to the magnetization direction of the magnet, magnetic-field generation appears in different shapes. Because of the ferromagnetic structure located around the edge of the magnet, magnetic-flux-density gradient is generated in a slanted direction, not horizontal to the sidewall of the ferromagnetic structure. To effectively exploit the enhanced magnetic -flux-density gradient, microchannels need to be located in A area rather than B, in (a) and (b), respectively. c) Experimental setup of a microfluidic device and a permanent magnet and an inverted microscope. Dark-circled edges of ferromagnetic structures in (a–c) depict highly converged points of magnetic-flux lines while open circles represent the depletion of the flux lines.

Experimental setup for magnetophoretic separation: Microfluidic devices were mounted on an inverted microscope (TS100; Nikon, Japan) and sample solution was attentively manipulated by a syringe pump (PHD22/2000; Harvard Apparatus, MA, USA). A permanent magnet (NdFeB35, 50 mm × 25 mm × 10 mm; Magtopia, Korea) was positioned near to the nickel microstructure. As shown in Figure 9, the geometric arrangement between a permanent magnet and a microfluidic device containing the ferromagnetic structure is a significant factor in the effective magnetophoresis of superparamagnetic particles. According to the geometric position as given in Figure 9a and b, magnetic flux lines converge at dark-circled edges and magnetic-flux density becomes minimized at open-circled edges. To achieve successful magnetophoretic separation, B and ∇B are important parameters, as given by F_{mag} (Equation (1)). With a given permanent magnet, the edges of the magnet offer highly converged magnetic-flux density, which consequently gives rise to the stronger magnetic force. However, the magnetic-flux lines around the edges of the magnet generally form in a direction diagonal to the overall shape of the magnet. Therefore, the geometric position of three compartments (microchannels, ferromagnetic nickel structure, and permanent magnet) should be arranged as presented in Figure 9c to utilize the highest magnetic force at the edges generating a magnetic-field gradient across the microchannel. The reason that we designed the separation microchannel and the nickel structure to be 2.5 cm in length (the same width of the permanent magnet) also arose from the use of the edge magnetic field. The as-dispersed SWCNT solution was drawn into the microfluidic channel by a syringe pump at a mass flow rate of 0.36 mg h^{-1} for 2–3 days. The single purification process took quite a long time to obtain a sufficient amount of the purified sample for purity assay, which requires careful and precise handling of the microfluidic system. The samples collected at the outlets were followed by further analysis to validate the purity of the purified samples.

Surfactant removal from SWCNTs: The collected SWCNT solution from each outlet was dried by evaporating water and surfactants were washed out using methanol solution. To remove the surfactant molecules attached to SWCNTs, the methanol-washed SWCNTs were heated at 200° C for 13 h.

SWCNTs analysis: The metal impurity and quality of SWCNTs were analyzed by EDS (XL30SFEG; Philips), TGA (Setsys 16/18; Setaram), and SQUID magnetometry (MPMS5; Quantum Design). The SWCNT samples for TGA were heated in air (30 sccm) to 1000 °C at the increasing rate of 5 °C min^{-1} with a stabilizing time of 10 min at 100 °C.

Acknowledgements

This work was supported by the Nano/Bio Science & Technology Program (M10536090002-05N3609-00210, M10503000218-05M0300-21810) of the Ministry of Science and Technology (MOST), and by the CHUNG Moon Soul Center for BioInformation and BioElectronics, Korea. The authors acknowledge Prof. Jeong Yong Lee for the TEM images. The TGA and EDS studies were supported by KAIST Research Supporting Team, and the SQUID results were obtained by Korea Basic Science Institute (KBSI).

[1] K. Wang, H. A. Fishman, H. Dai, J. S. Harris, *Nano Lett.* **2006**, *6*, 2043 – 2048.
[2] Z. Chen, J. Appenzeller, Y.-M. Lin, J. Sippel-Oakley, A. G. Rinzler, J. Tang, S. J. Wind, P. M. Solomon, P. Avouris, *Science* **2006**, *311*, 1735.
[3] Y.-Q. Xu, H. Peng, R. H. Hauge, R. E. Smalley, *Nano Lett.* **2005**, *5*, 163 – 168.
[4] S. R. C. Vivekchand, R. Jayakanth, A. Govindaraj, C. N. R. Rao, *Small* **2005**, *1*, 920 – 923.
[5] F. Chen, Y. Xue, V. G. Hadjiev, C. W. Chu, P. Nikolaev, S. Arepalli, *Appl. Phys. Lett.* **2003**, 83, 4601 – 4603.
[6] Y. Kim, D. E. Luzzi, *J. Phys. Chem. B* **2005**, *109*, 16636 – 16643.
[7] L. Thiên-Nga, K. Hernadi, E. Ljubović, S. Garaj, L. Forró, *Nano Lett.* **2002**, *2*, 1349 – 1352.
[8] D. E. Johnston, M. F. Islam, A. G. Yodh, A. T. Johnson, *Nat. Mater.* **2005**, *4*, 589 – 592.
[9] X. Li, K. G. Klemic, M. A. Reed, F. J. Sigworth, *Nano Lett.* **2006**, *6*, 815 – 819.
[10] E. M. Chan, R. A. Mathies, A. P. Alivisatos, *Nano Lett.* **2003**, *3*, 199 – 201.
[11] G. M. Whitesides, *Nature* **2006**, *442*, 368 – 373.
[12] P. S. Dittrich, K. Tachikawa, A. Manz, *Anal. Chem.* **2006**, *78*, 3887 – 3908.
[13] J.-U. Park, M. A. Meitl, S.-H. Hur, M. L. Usrey, M. S. Strano, P. J. A. Kenis, J. A. Rogers, *Angew. Chem. Int. Ed.* **2006**, *45*, 581 – 585.
[14] L. Larrimore, S. Nad, X. Zhou, H. Abruña, P. L. McEuen, *Nano Lett.* **2006**, *6*, 1329 – 1333.
[15] Q. Fu, J. Liu, *J. Phys. Chem. B* **2005**, *109*, 13406 – 13408.
[16] M. H. Moon, D. Kang, J. Jung, J. Kim, *J. Sep. Sci.* **2004**, 27, 710 – 717.
[17] H. Peng, N. T. Alvarez, C. Kittrell, R. H. Hauge, H. K. Schmidt, *J. Am. Chem. Soc.* **2006**, *128*, 8396 – 8397.
[18] a) K. S. Kim, J.-K. Park, *Lab Chip* **2005**, 5, 657 – 664; b) Y. K. Hahn, Z. Jin, J. H. Kang, E. Oh, M.-K. Han, H.-S. Kim, J.-T. Jang, J.-H. Lee, J. Cheon, S. H. Kim, H.-S. Park, J.-K. Park, *Anal. Chem.* **2007**, *79*, 2214 – 2220.
[19] N. Pamme, C. Wilhelm, *Lab Chip* **2006**, 6, 974 – 980.
[20] J. A. Oberteuffer, *IEEE Trans. Magn.* **1973**, *9*, 303 – 306.
[21] N. Xia, T. P. Hunt, B. T. Mayers, E. Alsberg, G. M. Whitesides, R. M. Westervelt, D. E. Ingber, *Biomed. Microdevices* **2006**, 8, 299 – 308.
[22] H. Lu, M. A. Schmidt, K. F. Jensen, *Lab Chip* **2005**, 5, 23 – 29.
[23] S. Zaric, G. N. Ostojic, J. Kono, J. Shaver, V. C. Moore, R. H. Hauge, R. E. Smalley, X. Wei, *Nano Lett.* **2004**, *4*, 2219 – 2221.
[24] G. Cliff, G. W. Lorimer, *J. Microsc.* **1975**, 103, 203 – 207.
[25] M. F. Islam, E. Rojas, D. M. Bergey, A. T. Johnson, A. G. Yodh, *Nano Lett.* **2003**, *3*, 269 – 273.

Received: May 14, 2007
Revised: July 14, 2007

